PHOTOELASTIC CALIBRATION OF TORSION SHAFTING

JAMES K. HAMEL

PHOTOELASTIC CALIBRATION

OF TORSION SHAFTING

by

James K. Dantel

PHOTOELASTIC CALIBRATION OF TORSION SHAFTING

by

James K. Hamel
//
Lieutenant, United States Navy

Submitted in partial fulfillment of
the requirements for the degree of

MASTER OF SCIENCE

IN

MECHANICAL ENGINEERING

United States Naval Postgraduate School
Monterey, California

1 9 6 0

PHOTOELASTIC CALIBRATION OF TORSION SHAFTING

by

James K. Hamel

This work is accepted as fulfilling

the thesis requirements for the degree of

MASTER OF SCIENCE

IN

MECHANICAL ENGINEERING
from the
United States Naval Postgraduate School

Abstract

This thesis is a presentation of the photoelastic technique for stress analysis applied to transmission shafting. Experimental effort was directed to devise a unique photoelastic sleeve which, when bonded to the reflective surface of a shaft, would provide a direct indication of shaft torque. A suitable stress-optic material molded to a working shaft makes this method useful for practical application.

The writer wishes to express his appreciation for the assistance and encouragement given to him by Professor R. E. Newton of the United States Naval Postgraduate School.

Symbols

R	Relative retardation (wavelengths)
C	Material Fringe Constant (fringe/psi)
δ	Thickness of Plastic (inches)
σ_1	Principal Stress (psi)
σ_2	Principal Stress (psi)
n	Fringe Order
λ	Wavelength of Monochromatic Green (21.5×10^{-6} in.)
E	Modulus of Elasticity (psi)
G	Shear Modulus (psi)
μ	Poisson's Ratio
K	Material Fringe Constant (fringe-inch/inch)
$\mathring{A}$	Angstrom Units (10^{-8} cm.)
J	Polar Moment of Inertia ($in.^4$)
ϵ_1	Principal Strain (micro-inch/inch)
ϵ_2	Principal Strain (micro-inch/inch)
M_t	Twisting Moment (inch-pounds)
M_b	Bending Moment (inch-pounds)
a	Inner Radius of Plastic Sleeve (inches)
x	Distance from Thin Edge of Plastic Sleeve to Fringe Location (inches)
$2\backslash^{-3}$	2×10^{-3}

Table of Contents

List of Illustrations

List of Tables

1. Introduction

The photoelastic method of experimental stress analysis as developed and introduced to the engineering world in 1930 by Professor E. G. Coker and L. N. G. Filon in their "Treatise on Photoelasticity" was but a qualitative approach to the complex problem of mathematical stress analysis in which the theory of elasticity and stress functions are employed. Since that time, many improvements in photoelastic technique, materials and equipment, have placed the method in a category where:

> Today photoelasticity has grown to the full stature of a powerful technical instrument of quantitative stress analysis which for two dimensions, at least, exceeds all other methods in reliability, scope and practicability. There is no method by which the complete exploration of principal stresses, let alone the stress on free boundaries, can be determined with the same speed and accuracy and at such a surprising small cost as the photoelastic method. Nor is there a method which has the same visual appeal and covers so much of the stress field with one pattern.[1]

Photoelastic analysis generally requires the construction of a model geometrically similar to the part being analyzed. These models are made of materials possessing the property of stress-optic sensitivity.[2] More recently, however, a doubly refracting plastic, which can be bonded directly to an actual part under study, was developed. It is marketed under the trade name Photostress Plastic. Strains in the actual part produce equal strains in the plastic. In turn, the plastic exhibits birefringence which may be studied by standard photoelastic techniques.[3] The method makes two dimensional studies of actual structures practical.

---

[1] M. M. Frocht, Photoelasticity, Vol. 1, Preface, Wiley & Sons, 1941.
[2] Ibid., Chapter 10.
[3] Felix Zandman, Photostress Analysis, Product Engineering, p 5, March 2, 1959.

This investigation is an application of the photoelastic method to devise a permanent, continuous and direct reading torque meter for transmission shafting. Of particular interest is slowly rotating shafting, such as ship propellor shafts, where stroboscopic illumination is not feasible. Shafting of this nature, ideally in a condition of pure torsional shear producing stresses which are everywhere the same on the surface, presents a problem well suited for experiment. One method of solution measures retardation due to double refraction with a Babinet compensator. This refraction is produced in a uniform Photostress sleeve bonded to a shaft.[1] A tapered photoelastic sleeve as shown in Fig. 1, would eliminate the necessity for a compensator. Using monochromatic illumination, the tapered sleeve arrangement, when strained, produces a direct reading pattern of circumferential isochromatics along the length of the sleeve (Fig. 2). The spacing of these isochromatics provides a direct measure of the torque and torque measurements can be made regardless of shaft speed.

The effect of bending moment on the stress-optic pattern produced by torsion is also considered in this investigation. In machinery installations, bending moment is always present to some degree due to misalignment or shaft dead weight.

---

[1]Felix Zandman, Photostress Analysis, Product Engineering, p.5, March 2, 1959.

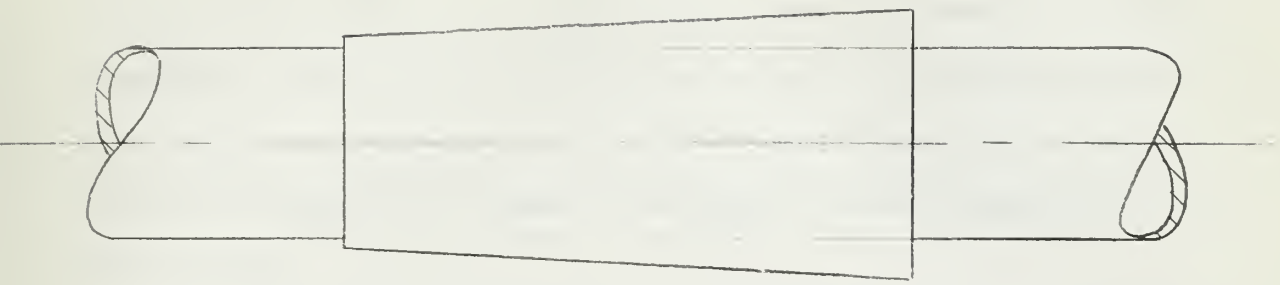

Fig. 1. A Tapered Photoelastic Sleeve
Bonded to a Torsion Shaft.

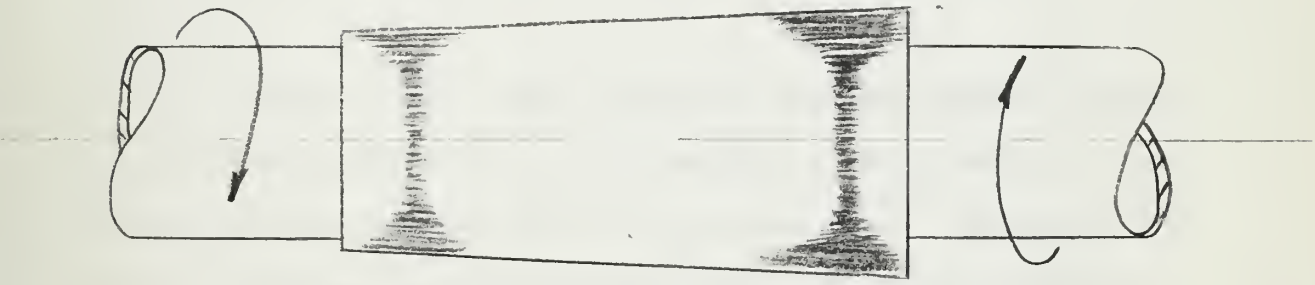

Fig. 2. Photoelastic Pattern Developed
in Torqued Shaft Sleeve.

2. Stress-Optic Effects

The stress-optic effect is the temporary double refraction produced in an isotropic body subjected to stress. Upon removal of loads producing the condition of stress within a body, the double refraction disappears. The planes of principal stress act as polarizing planes along which the components of light are allowed to pass and become refracted or stepped out of phase in accordance with the stress-optic law which states:

> In a transparent isotropic plate in which the stresses are two-dimensional and within the elastic limit, the phase difference or relative retardation R, in wavelengths, between the rectangular wave components traveling through it and produced by temporary double refraction is given by
>
> $$R = C \delta (\sigma_1 - \sigma_2) \qquad (1)$$
>
> in which C is a constant known as the stress-optic coefficient, δ is the thickness of the plate, and σ_1 and σ_2 are the principal stresses.[1]

The relation between the relative retardation and the stresses producing temporary refraction in a transparent isotropic body is empirical.[2]

The transverse wave theory adequately describes optical phenomena associated with polarization and stress-optic effects, and can be used to describe the effects achieved in this experiment.[3] The system producing the desired experimental stress-optic effects was equivalent to a bright field plane polariscope and was chosen because it easily

---

[1] M. M. Frocht, Photoelasticity, Vol. 1, p. 136, Wiley & Sons, 1941.

[2] Coker & Filcon, Treatise on Photoelasticity, Chap. 3, Cambridge University Press, London.

[3] Ibid., 1. Chap 3.

adapted to the problem of transmission shafting.

Consider a horizontal shaft with a photoelastic sleeve bonded to its reflective surface. A single Polaroid sheet (axis of polarization perpendicular to longitudinal tube axis) serves as polarizer and analyzer. Light from a monochromatic source passes through the Polaroid and the plastic sleeve; it is then reflected from the shaft surface and travels back through the plastic and the Polaroid, to the eye of the observer.

When the shaft is subjected to torsion, the strain developed on the surface of the tube will impart equal strains to each infinitesimal area of the sleeve bonded to it. Light passing through the polariscope system mounted on the shaft will be refracted in the plastic sleeve as a result of these strains. Viewed under monochromatic illumination, a point of the sleeve will pass cyclically from maximum brightness to darkness to maximum brightness as the principal stress difference is increased. Since the relative retardation is proportional to thickness, a tapered sleeve such as shown in Fig. 1, will exhibit a pattern of circumferential isochromatics. Note that the effective thickness of the plastic sleeve at any point along its length is double the actual thickness, since reflected light necessarily passes through the plastic a second time.

In a bright field plane polariscope, the dark fringes observed are of order $n = 1/2, 3/2, 5/2, \ldots$ .Then $R = n\lambda$, where λ is the wavelength of the light used. Referring to Eq. 1, we see that the principal stress difference $\sigma_1 - \sigma_2$ may be found. From this stress difference the shaft torque is readily determined.

The simplicity of such a system is obvious. Once installed, it becomes a permanent part of the equipment; the only auxiliary items required to determine torque are a monochromatic light source, and some suitable scale for measuring the stress-optic pattern.

3. Static Photoelastic Calibration of the Test Shaft

The test shaft used in this experiment was a seamless aluminum alloy tube of dimensions and properties given in Table I.

Table I

Properties of 2024S-T3 Aluminum Alloy[1]	
Outside Diameter, D_o	1.002 inches
Wall thickness, t	0.0355 inches
Modulus of Elasticity, E_t	10.6×10^6 psi
Shear Modulus, G_t	4.00×10^6 psi

The tube dimensions were carefully measured with micrometer calipers. The modulus of elasticity, as given by the Alcoa Structural Handbook, was corroborated by independent tension tests, using a test section of the 2024 aluminum alloy tube and SR-4 strain gages. On this basis the shear modulus was assumed correct as listed.

Next a determination of the pertinent physical properties of the Photostress Type A plastic was required. Details of the technique for fabricating the plastic sleeve are given in Appendix III. When the final plastic sleeve was fabricated, enough liquid was reserved from the batch to make two tensile specimens similar to those shown in Fig. 17, providing two test bars of exactly the same composition. The first of these bars was inserted into the field of a Chapman plane polariscope, loaded axially in tension, and the material fringe constant determined. A detailed description of this experiment, along with experimental data, is given in Appendix I.

[1] Alcoa Structural Handbook, Table of Properties, p. 34, 1955.

On the second of the test bars, two Tuckerman optical strain gages were mounted. These two strain gages occupied positions on opposite sides of the bar; one mounted along the longitudinal bar axis and the other mounted laterally. Then, for each known increment of axial tension load applied, the longitudinal and lateral strains were observed. From these observations the modulus of elasticity, the shear modulus, and Poisson's ratio were determined. A detailed description of this experiment and the resulting data are given in Appendix II.

The results of the experiments described in Appendices I and II are tabulated below:

Table II

Properties of Photostress Type A Liquid Plastic	
Modulus of Elasticity, Ep	445,000 psi
Shear Modulus, G_p	152,000 psi
Poisson's Ratio, μ	0.46
Material Fringe Constant, K^1	0.0829 fringe-inch/inch

The necessary physical constants of the materials used having been determined, actual system calibration began. For this purpose, a jig was fabricated (Fig. 3) which could provide various combinations of torque and bending simultaneously to the test shaft. The jig consisted of two knife edges which supported the test shaft horizontally. Located an equal distance outside each knife edge was a split disc or flange clamped to the test shaft for the purpose of transmitting torque to the shaft. These flanges were fitted with horizontal lever arms,

[1] See Appendix II.

extending in opposite directions perpendicular to the tube length, from which dead weights could be suspended. With a given load suspended from the lever arms, the torque transmitted to the test shaft could be varied, depending on the location of the dead weight along the lever length. Bending moment remained constant through a run and was determined by the product of load applied and the distance from flange to knife edge.

Fig. 3 Jig used for static calibration with monochromatic mercury vapor source and barrel sight.

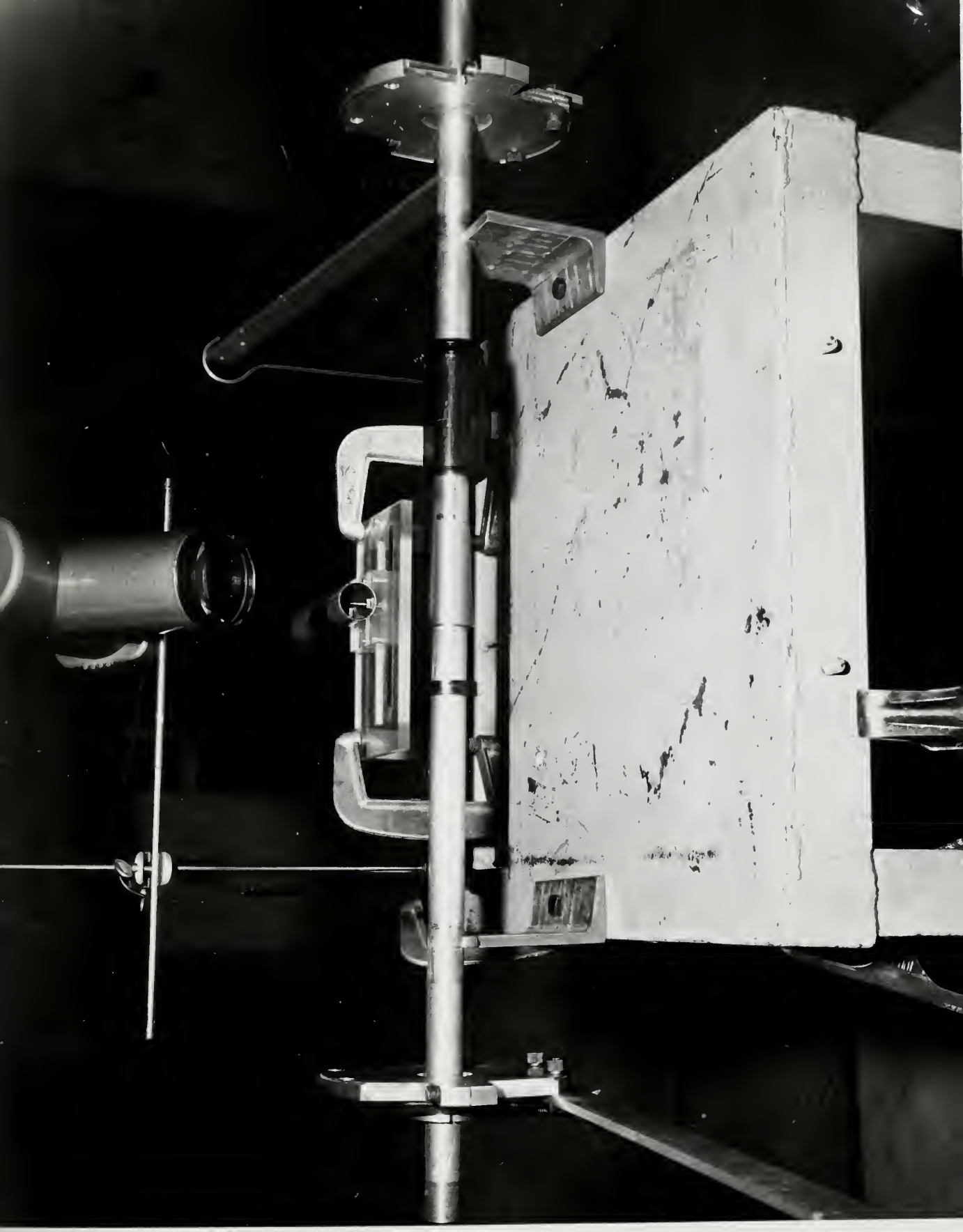

Fig. 4 Exploded view of sleeve and Polaroid sheet. Seen in greater detail is the barrel sight.

Primary illumination, a monochromatic green light (5461Å = 21.5 x 10^{-6} inches), was achieved with a mercury vapor lamp and suitable filter (Fig. 4). The primary illumination was supplemented by ordinary stray white daylight. In subsequent experimental work, the stray white light was found to aid substantially in locating low order fringes. The white light, alone, produced too diffuse a pattern to use quantitatively.

The device used to measure the stress-optic pattern developed in the torsion bar sleeve was a simple cross hair sighting barrel (Figs. 3 and 4). To the barrel was attached a pointer matched to a six inch scale. The barrel, set in tracks parallel to the long tube axis, moved parallel to the tube and was used to measure the distance, x, from the thin edge of the sleeve to a fringe location. Readings taken in this manner could be reproduced to within $\pm$ 0.02 inches.

Figures 3 and 4 also show the method employed to fix the polarizer-analyzer combination in place. The Polaroid forms an outer sleeve over the plastic (shown in an exploded view in Fig. 4) which is bound on the ends to solid discs placed to prevent end light leakage.

The first calibration runs were performed to confirm system linearity. With the flanges of the torsion jig fixed adjacent to the supports (to avoid all but a minimum of bending moment), the lever arms were loaded, in increments, from zero to 1015 inch pounds. This loading closely approximated a condition of pure torsional shear.

For the aluminum tube: r_o = 0.501 in., r_i = 0.4655 in.. The torsional rigidity is

$$(GJ)_t = G\frac{\pi}{2}\left(r_o^4 - r_i^4\right) = 10.1^{\backslash 4} \text{ lb-in}^2$$

where J is the polar moment of inertia (in^4). For the plastic sleeve: a = 0.501 in., $\delta = 0.042 + 0.048\ x$, $G_p = 152{,}000$ psi. The subscripts t and p refer to the aluminum tube and the plastic sleeve respectively.

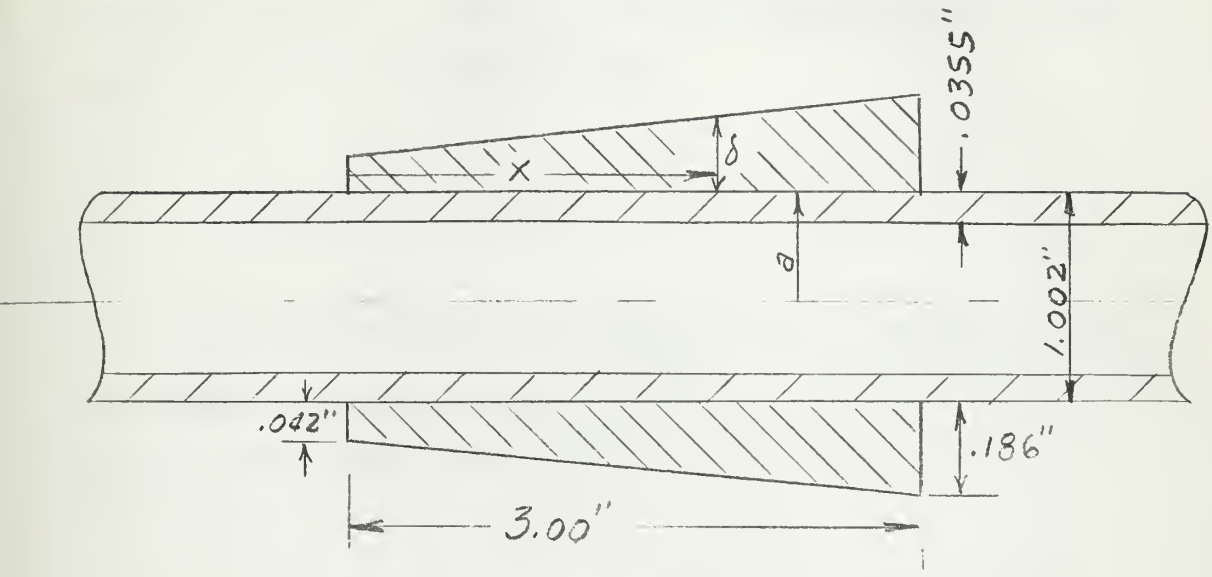

FIG. 5 TUBE-SLEEVE CROSS SECTION

An alternate form of the stress-optic equation states:[1]

$$n\lambda = 2K\delta(\epsilon_1 - \epsilon_2) \tag{2}$$

where ϵ_1 and ϵ_2 are the principal strains. The principal strain difference is equal to the maximum shearing strain γ_{max}. At a radius r

$$\epsilon_1 - \epsilon_2 = \gamma_{max} = r\,\vartheta \tag{3}$$

[1] See Appendix II.

where θ is the angle of twist per unit length. It is well known that[1]

$$\theta = \frac{M_t}{GJ} \tag{4}$$

where M_t is the twisting moment and GJ is the torsional rigidity. Torsional rigidity is made up of the contributions of both the tube (shaft) and plastic sleeve,[2] so that

$$GJ = (GJ)_t + (GJ)_p \tag{5}$$

At a location where the sleeve thickness is δ (see Fig. 5), the mean radius r of the sleeve is $a + \delta/2$. Using this value, and the results of Eqs. 4 and 5, Eq. 3 gives

$$\epsilon_1 - \epsilon_2 = \frac{M_t}{(GJ)_t + (GJ)_p}\left(a + \delta/2\right)$$

Inserting this in Eq. 2 and solving for n/M_t yields

$$\frac{n}{M_t} = \frac{2k\delta}{\lambda} \cdot \frac{(a + \delta/2)}{\left[(GJ)_t + (GJ)_p\right]} \tag{6}$$

Values of n/M_t from Eq. 6 for various values of x (see Fig. 7) are given in Table III.

---

[1] Timoshenko, Str. Materials, Part I, p. 283, 3rd Ed., Van Nostrand, New York, 1955.

[2] In normal applications the plastic sleeve will make a negligible contribution.

Table III

Calculated values of fringe order per unit torque n/M_t.

x	δ	$(GJ)_p + (GJ)_t^-$	n/M_t
inches	inches	pound-inches	
0	0.042	$10.64\backslash^{4}$	$1.58\backslash^{-3}$*
1	0.090	$11.51\backslash^{4}$	$3.29\backslash^{-3}$
2	0.138	$12.57\backslash^{4}$	$4.83\backslash^{-3}$
3	0.186	$13.90\backslash^{4}$	$6.12\backslash^{-3}$

* $1.58\backslash^{-3} = 1.58 \times 10^{-3}$, etc.

Table IV

Experimentally observed fringe locations.

x	n	M_t	n/M_t
inches		inch-pounds	
0.75	1/2	190	$2.63\backslash^{-3}$
1.57	3/2	355	$4.23\backslash^{-3}$
0.84	3/2	520	$2.88\backslash^{-3}$
1.95	5/2	520	$4.81\backslash^{-3}$
0.47	3/2	685	$2.19\backslash^{-3}$
1.25	5/2	685	$3.65\backslash^{-3}$
2.20	7/2	685	$5.11\backslash^{-3}$
0.24	3/2	850	$1.76\backslash^{-3}$
0.84	5/2	850	$2.94\backslash^{-3}$
1.55	7/2	850	$4.12\backslash^{-3}$
2.31	9/2	850	$5.29\backslash^{-3}$
0.58	5/2	1015	$2.46\backslash^{-3}$
1.16	7/2	1015	$3.45\backslash^{-3}$
1.75	9/2	1015	$4.43\backslash^{-3}$
2.45	11/2	1015	$5.41\backslash^{-3}$

Calculated results contained in Table III are plotted as the solid curve of Fig. 7. The experimentally observed points given in Table IV are also shown. The agreement between calculated and experimental values is obvious.

Figure 6 below, indicates a typical sleeve pattern under load conditions of torsional shear.

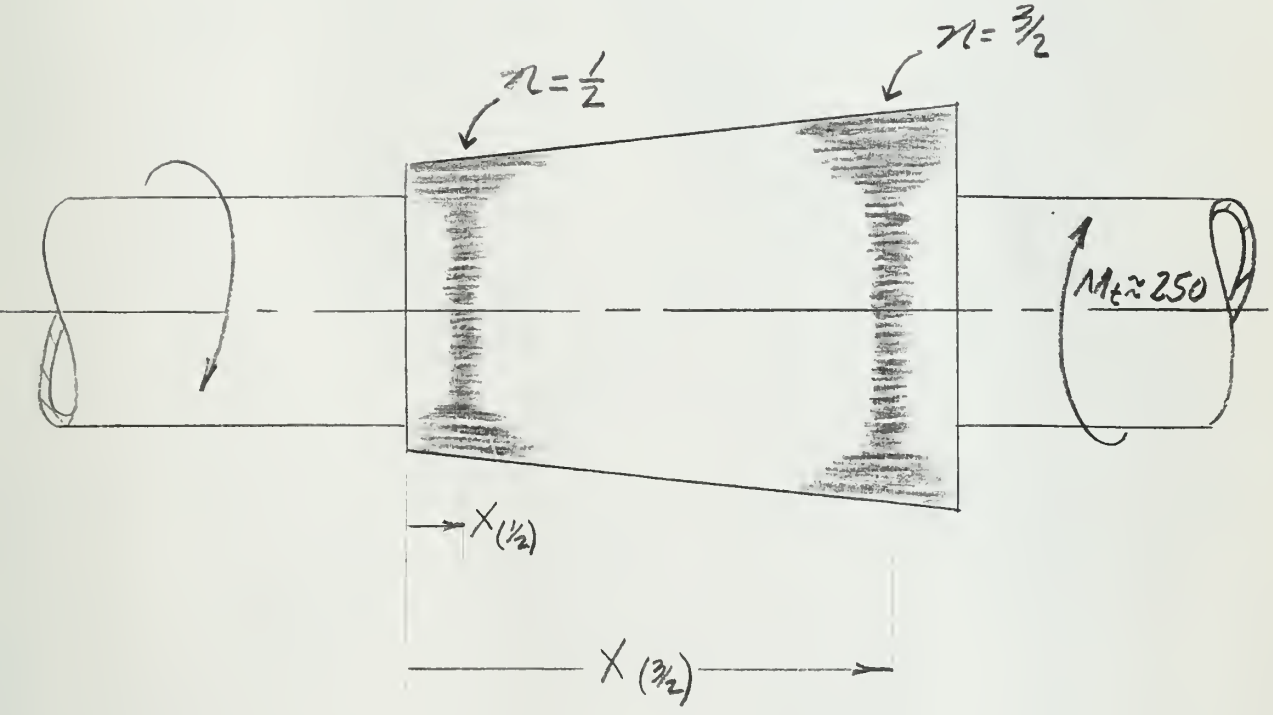

Fig. 6. Typical sleeve pattern developed with shaft subject to torsion.

STATIC TEST
FRINGE ORDER PER UNIT TORQUE
VS DISTANCE X
FOR THE CASE OF FIG. 7
TORSION W/O BENDING

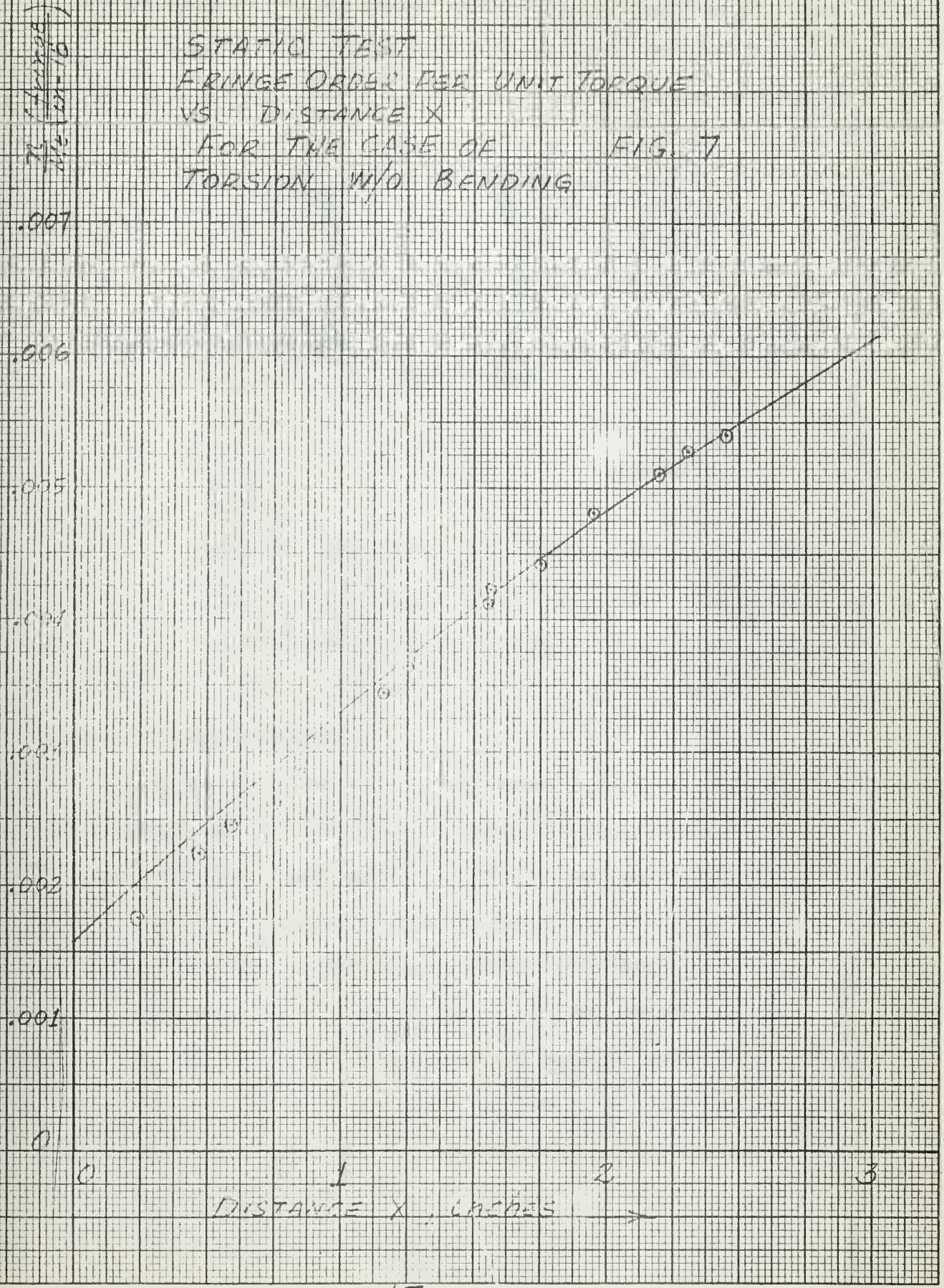

The presence of bending moments distorts the isochromatic pattern (Fig. 8). If the bending moment vector rotates with the shaft the pattern will also rotate. If the rotative speed is high it may be possible

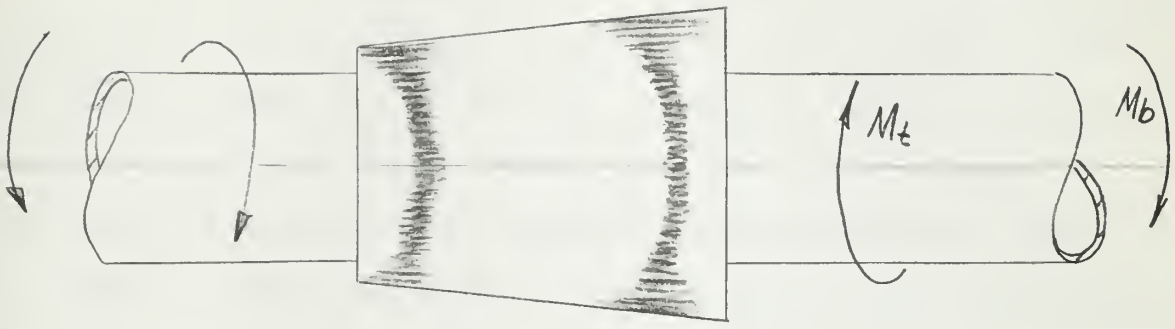

Fig. 8. The effect of bending on the stress-optic pattern.

to study the fringes with stroboscopic illumination, but at low speeds this is not feasible. On the other hand, if the bending moment vector is stationary the isochromatic pattern will also be stationary. This latter situation occurs when the bending moments result from either gravity loads or bearing misalignment.

A separate set of static tests was performed to study the effect of bending moments on the isochromatic pattern. The results of these tests were also found to be reproducible to within close limits over several runs ($\Delta x = \pm 0.02$ inches). Readings taken along the neutral surface (where the effects of bending stresses are absent) for this combined system were precisely those given, within the limits stated, in Table IV for similar torque conditions. For bending, readings of fringe location are taken 90° from the neutral surface on the compression or tension side of the test bar. In this experiment, readings were taken

on the upper or tension side.

The theory already developed for predicting the isochromatic pattern for pure torsion is readily extended to the combined loading. The isochromatic fringe order is directly proportional to the maximum shearing stress at the surface of the shaft and this, in turn, is proportional to the resultant moment $M = \sqrt{M_t^2 + M_b^2}$, where M_t is the torsional moment and M_b is the bending moment. This result is a well-known consequence of applying the maximum shear theory of failure to a shaft under such a combination loading.[1] Substituting this result in Eq. 6 gives

$$\frac{n}{\sqrt{M_t^2 + M_b^2}} = \frac{2K\delta}{\lambda} \cdot \frac{(\sigma + \delta/2)}{\sqrt{(\sigma + \delta/2)^2 + \tau^2}} \qquad (6')$$

In Table V experimentally observed values of fringe position are given, along with corresponding values of $n/\sqrt{M_t^2 + M_b^2}$. In Fig. 9 these results are plotted as circled points and the solid theoretic curve has been calculated from Eq. 6'.

Tests conducted over a six hour period, with constant load applied to the test bar, had no apparent effect on the stress-optic pattern, and fringe location did not vary detectably over the load period. It was, therefore, assumed that the creep properties of the plastic, or a stress relaxation effect, did not enter the problem.

---

[1] See, for example, Timoshenko, Str. of Materials, Part II, p 447, 3rd Ed., Van Nostrand, New York, 1955. There is a minor error committed when this result is applied to a nonhomogeneous shaft made from materials having different Poisson's ratios. The error is unimportant in practical situations.

Table V

Experimentally observed values of fringe location x.

x inches	n	M_t in-lb	M_b in-lb	$n/\sqrt{M_t^2 + M_b^2}$
0.30	3/2	685	150	2.14×10^{-3}
1.09	5/2	685	150	3.57×10^{-3}
2.02	7/2	685	150	5.00×10^{-3}
0.10	3/2	850	150	1.74×10^{-3}
0.71	5/2	850	150	2.90×10^{-3}
1.42	7/2	850	150	4.06×10^{-3}
2.16	9/2	850	150	5.22×10^{-3}
0.46	5/2	1015	150	2.43×10^{-3}
1.03	7/2	1015	150	3.41×10^{-3}
1.63	9/2	1015	150	4.38×10^{-3}

STATIC TEST
FLANGE ORDER PER UNIT TORQUE
VS. DISTANCE X
FOR THE CASE OF TORSION WITH BENDING

Fig. 9

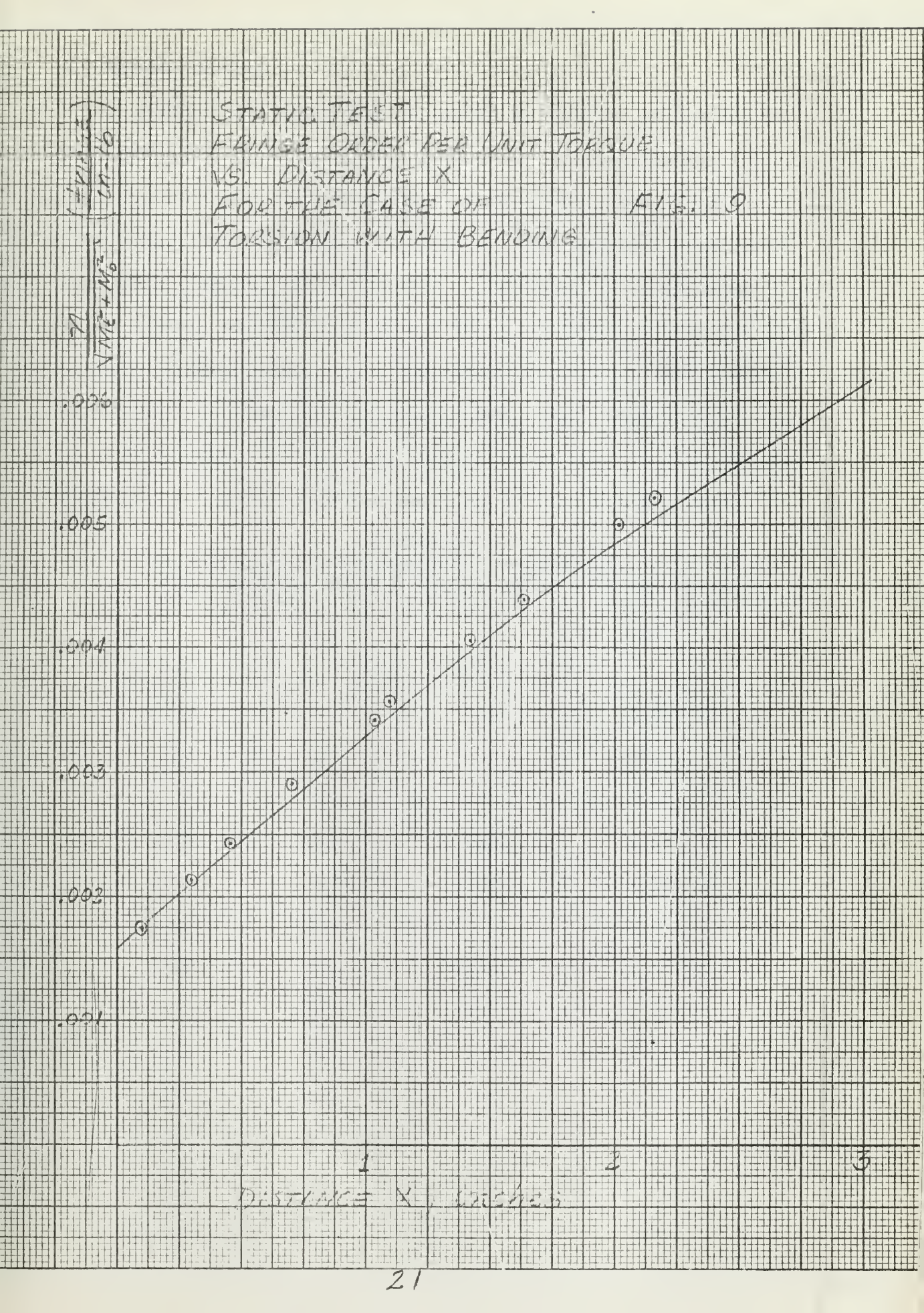

4. Dynamic Testing

A dynamic test simulating, as nearly as possible, actual service conditions, constituted the next test phase. For this purpose, the test shaft was made the driving shaft which linked a motor drive to a water brake loading system. The motor was instrumented to read driving torque directly, and was capable of providing 1015 inch pounds at speeds ranging from 200 to 400 rpm. The water brake provided 1015 inch pounds of braking torque at 400 rpm; lesser torques at lower speeds. The dynamic tests were run through the same torque range as the static calibration tests (0 to 1015 inch pounds) at as low a rotative speed as possible. The results obtained are given in the following table.

Table VI

Experimentally observed dynamic values of fringe location x.

x inches	n	M_t in-lb	n/M_t
0.76	1/2	190	3.00×10^{-3}
1.30	3/2	378	3.97×10^{-3}
0.56	3/2	567	2.65×10^{-3}
0.31	3/2	685	2.19×10^{-3}
0.23	3/2	756	1.98×10^{-3}
0.96	5/2	756	3.31×10^{-3}
2.08	7/2	685	5.12×10^{-3}
1.77	7/2	756	4.63×10^{-3}
1.48	7/2	850	4.12×10^{-3}
1.18	7/2	945	3.70×10^{-3}
1.83	9/2	945	4.76×10^{-3}
2.55	11/2	945	5.82×10^{-3}
2.30	11/2	1015	5.42×10^{-3}

Experimentally observed values of fringe order per unit torque n/M_t vs. fringe location x are shown plotted in Fig. 10 for comparison with the theoretical curve.

DYNAMIC TEST
FRINGE ORDER PER UNIT TORQUE
VS DISTANCE X

FIG. 10

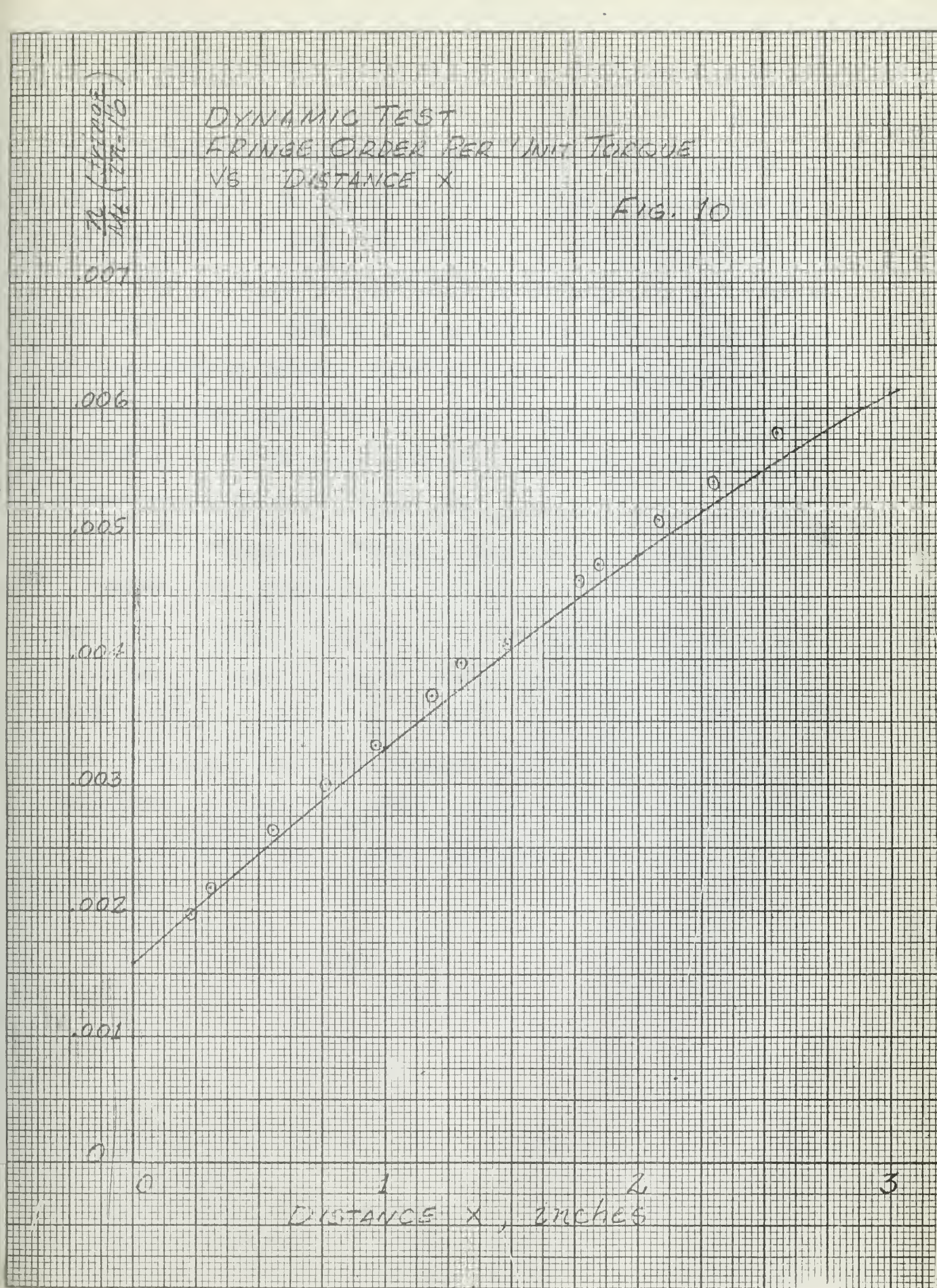

The dynamic testing further showed that bending moment, whose vector remains stationary in space, could be resolved as in the static test. In the case of this type of moment, the stress-optic pattern appears stationary, and the extreme limits of the fringe developed in the sleeve can be located. For bending moment due to shaft eccentricity, i.e., moment whose vector rotates with the shaft, resolution becomes impractical. For the speeds of rotation considered (200 to 400 rpm), the pattern appears to wobble so that quantitative measurement of fringe location is unreliable. While the dynamic test set up was not designed to study these effects specifically, sufficient shaft eccentricity was present and sufficient dead weight could be induced to note the effects of the resulting component stresses on the stress-optic pattern.

An alternative method for determining torque, when the stress-optic pattern developed presents two or more consecutive fringes, uses the distance between the fringes. Measuring distance between fringes would, in many instances, prove a simpler method because reference to the edge of the sleeve is not then required. The relation between torque M_t and distance separating consecutive fringes is shown in Fig. 11. Data used to construct this family of curves were derived from the theoretical curve of Fig. 7.

DISTANCE BETWEEN FRINGES VS TWISTING MOMENT M_t

FIG 11

FOR CONSECUTIVE FRINGES AS INDICATED

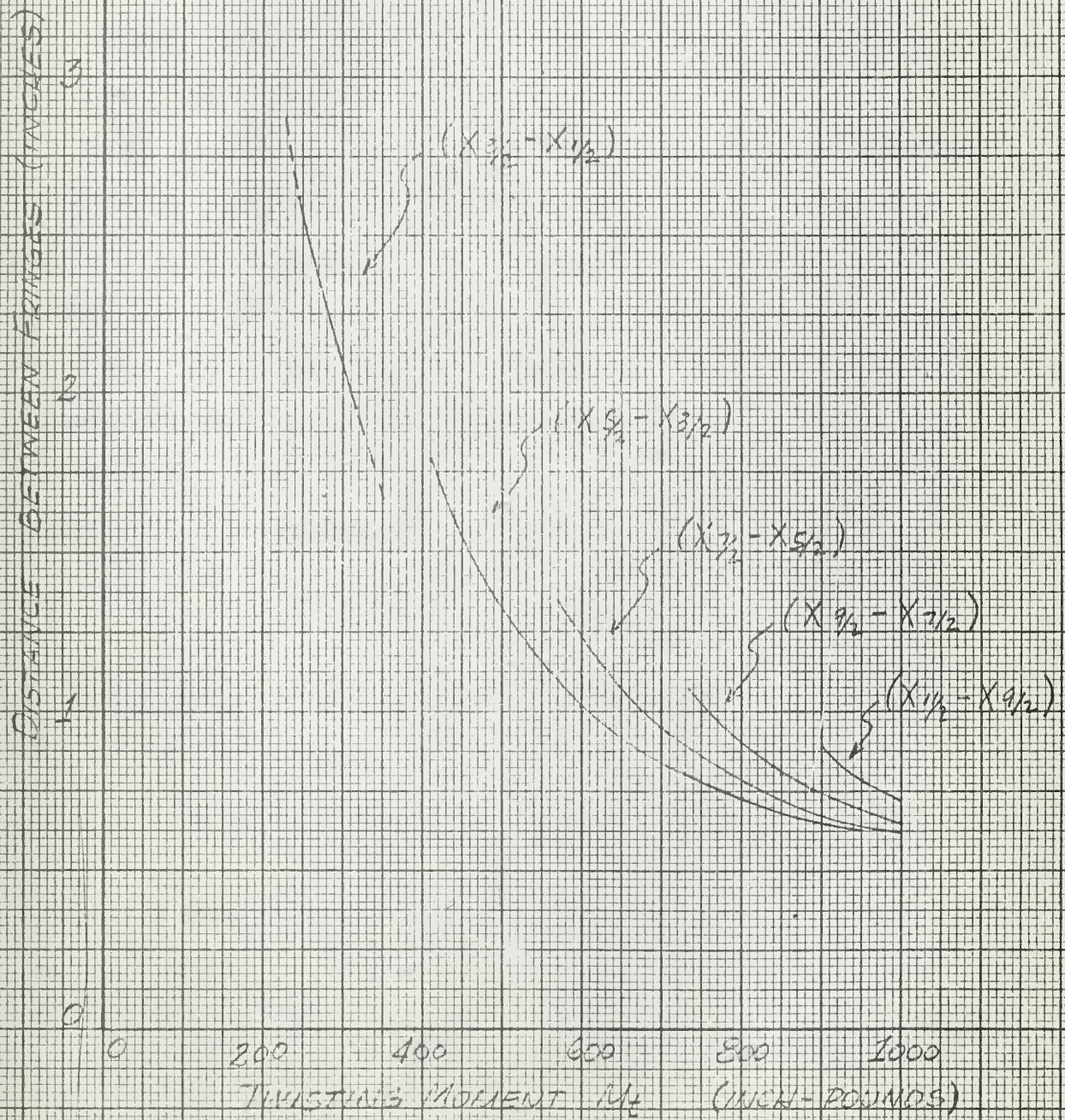

5. Conclusion

A knowledge of torque, as such, provides the engineer with a most useful quantity. Special complex equipment usually assembled for each test, and not normally considered part of the operating machinery, provides the customary approach to this determination. The results of this experimental work show that the photoelastic technique employed presents a simple and effective method for determining torque. Also, this photoelastic method, once applied, becomes a permanent part of the equipment and torque readings can be made directly and whenever desired.

It is important to note that the first fringe (n = 1/2) appearing in the photoelastic sleeve is diffuse, poorly defined, and virtually impossible to use for quantitative results under even darkroom conditions. As the 3/2 and higher order fringes appear, they are increasingly well defined for quantitative measure. A torque M_t of 190 inch pounds, the minimum increment of load in Table IV, causes the first fringe to appear and travel the length of the sleeve to the end effect zone. One hundred ninety inch pounds induces in the aluminum tube a shear stress of

In order to obtain a similar strain in a steel shaft, e.g., a ship propellor shaft, the corresponding stress would be approximately

A stress of this magnitude would seldom be encountered in ship shaft design practice.[1] It is obvious that in a system such as that used in this

[1] A Quarter Century of Propulsion Shafting Design Practice and Operating Experience in the U. S. Navy, Rudolph Michel, Design Division, Bureau of Ships, Washington, D. C.

experiment, either the first fringe must be used for quantitative measure or higher order fringes must be made to appear at low stress levels.

Higher order fringes can be developed at low stress levels by the use of more sensitive stress-optic material or by increasing the thickness of the photoelastic sleeve. Pending further developments in stress-optic materials, nothing more effective than Photostress is presently available for this particular use. However, the thickness of the sleeve may be increased to as much as 3/4 of an inch (with the linear dimensions increased proportionately). This would increase the response by a factor of four, making this system practical for the ship shaft application. It can be used conveniently in the main machinery spaces to observe: the increased torque output required to maintain a specified ship speed as the outer hull conditions fouled and deteriorated; turbine losses; and spring bearing losses. Other applications to shafts, large or small, regardless of rotative speed, can be made if torque determination is required, since the procedure requires only a small investment in time and money.

BIBLIOGRAPHY

1. M. M. Frocht, Photoelasticity, Wiley & Sons, 1941.

2. Coker & Filon, Treatise on Photoelasticity, Cambridge University Press, London, 1931.

3. Filon, A Manual of Photoelasticity for Engineers, Cambridge University Press, London, 1936.

4. M. Hetényi, The Fundamentals of Three Dimensional Photoelasticity, Journal of Applied Mechanics, Vol. 5, No. 4, December 1938, pp 41-49.

5. Felix Zandman, Photostress Analysis, Product Engineering, p 5, March 1959.

6. Perry & Lissner, The Strain Gage Primer, McGraw-Hill, New York, N. Y. 1955.

7. Alcoa, Alcoa Structural Handbook, Table of Properties, p 34, 1955.

8. Timoshenko, Str. of Materials, Part I, p 283, 3rd Ed., Van Nostrand, 1955.

9. Ibid, Part II, p 447.

10. Rudolph Michel, A Quarter Century of Propulsion Shafting Design Practice and Operating Experience in the U. S. Navy, Bureau of Ships, Washington, D. C.

11. American Instrument Company, Instruction for Tuckerman Optical Strain Gages.

12. B. L. Wilson, Characteristics of the Tuckerman Strain Gage, Proc. ASTM, Vol. 44, pp 1017-1026, 1944.

13. Lester H. Beck, A Photoelastic Investigation of Thermal Stresses, U. S. Naval Postgraduate School, 1958.

14. Newton R. E., A Photoelastic Study of Stresses in Rotating Discs, Journal Applied Mechanics, Vol. 7, No. 2, pp A57-60, 1940.

15. S. S. Redner, Tatnall Measuring Systems Company, Private Communication, October 1959.

16. Tatnall Measuring Systems Company, Photostress Bulletin PS-2060.

17. Tatnall Measuring Systems Company, Operating Instructions for Photostress L F/Z meter, Bulletin BN 8001, 1957.

18. Tatnall Measuring Systems Company, Instruction for Applying Photostress Sheet Plastic, Bulletin IB-8004, 1959.

19. Tatnall Measuring Systems Company, Instructions for Applying Photostress Liquid Plastic, Bulletin BN-8005, 1958.

20. Tatnall Measuring Systems Company, Instructions for Molding Contoured Sheets of Photostress Plastic, Bulletin IB-8008, 1958.

21. Tatnall Measuring Systems Company, Photostress Sheet and Liquid Plastic Suggestions for Plastic Selection, Bulletin BN-8002, 1959.

Appendix I

Photostress Type A Liquid Plastic

A Determination of the Material Fringe Value

In this experiment, a calibration model, cast and machined to size (Fig. 12), was loaded axially in tension in the field of a Chapman plane polariscope. Runs were made with both dark and light fields. Load applied to the model was measured with a Baldwin SR-4, type U, load cell connected to an SR-4, type N, strain indicator. The calibration model was strained until the ninth fringe order was observed.

Experimental data, charts, and calculations are shown on the following pages.

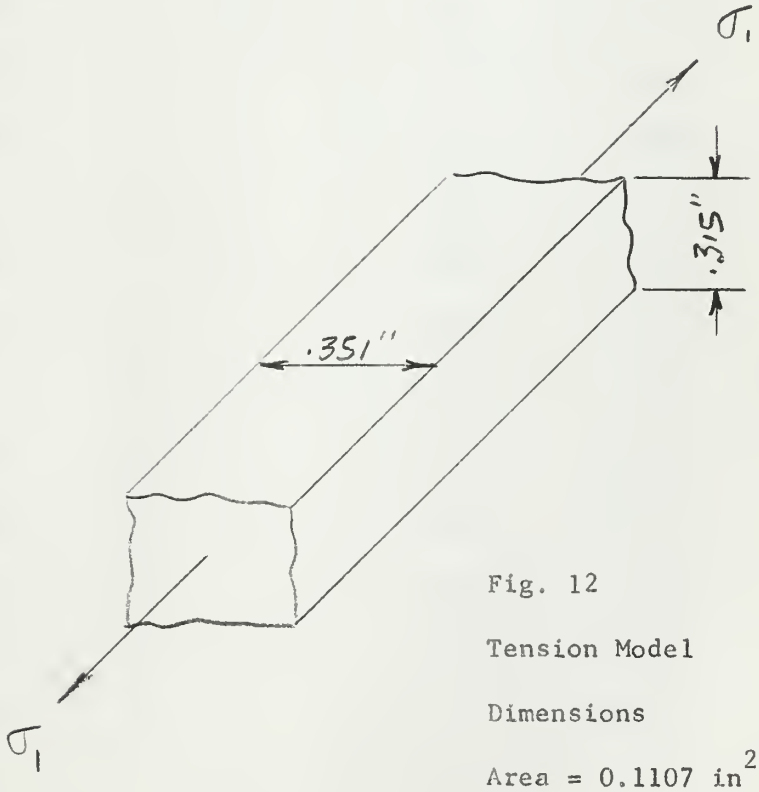

Fig. 12

Tension Model

Dimensions

Area = 0.1107 in^2.

Data

Photostress Type A Liquid Plastic---15 per cent Hardener by Weight

Tension Calibration and Determination of Material Fringe Value

Dark Field		Fringe Value	Light Field	
Load pounds	σ_1 psi		Load pounds	σ_1 psi
0	0	0	0	0
18.75	169.5	1	15.0	135.5
45.25	408	2	40.0	362
72.50	655	3	71.25	644
100.75	910	4	98.75	892
127.75	1152	5	127.0	1148
155.25	1403	6	153.25	1385
181.75	1641	7	179.50	1621
207.50	1872	8	205.25	1854
232.25	2100	9	231.25	2090
206.50	1868	8	209.75	1892
178.25	1611	7	181.25	1638
149.75	1352	6	154.25	1394
122.50	1108	5	121.75	1100
95.00	858	4	95.0	858
66.25	598	3	67.50	610
38.25	346	2	39.50	357
10.25	10.25	1	13.75	124.2
0	0	0	0	0

PHOTOSTRESS TYPE A LIQUID PLASTIC
STRESS VS FRINGE ORDER

Fig. 13

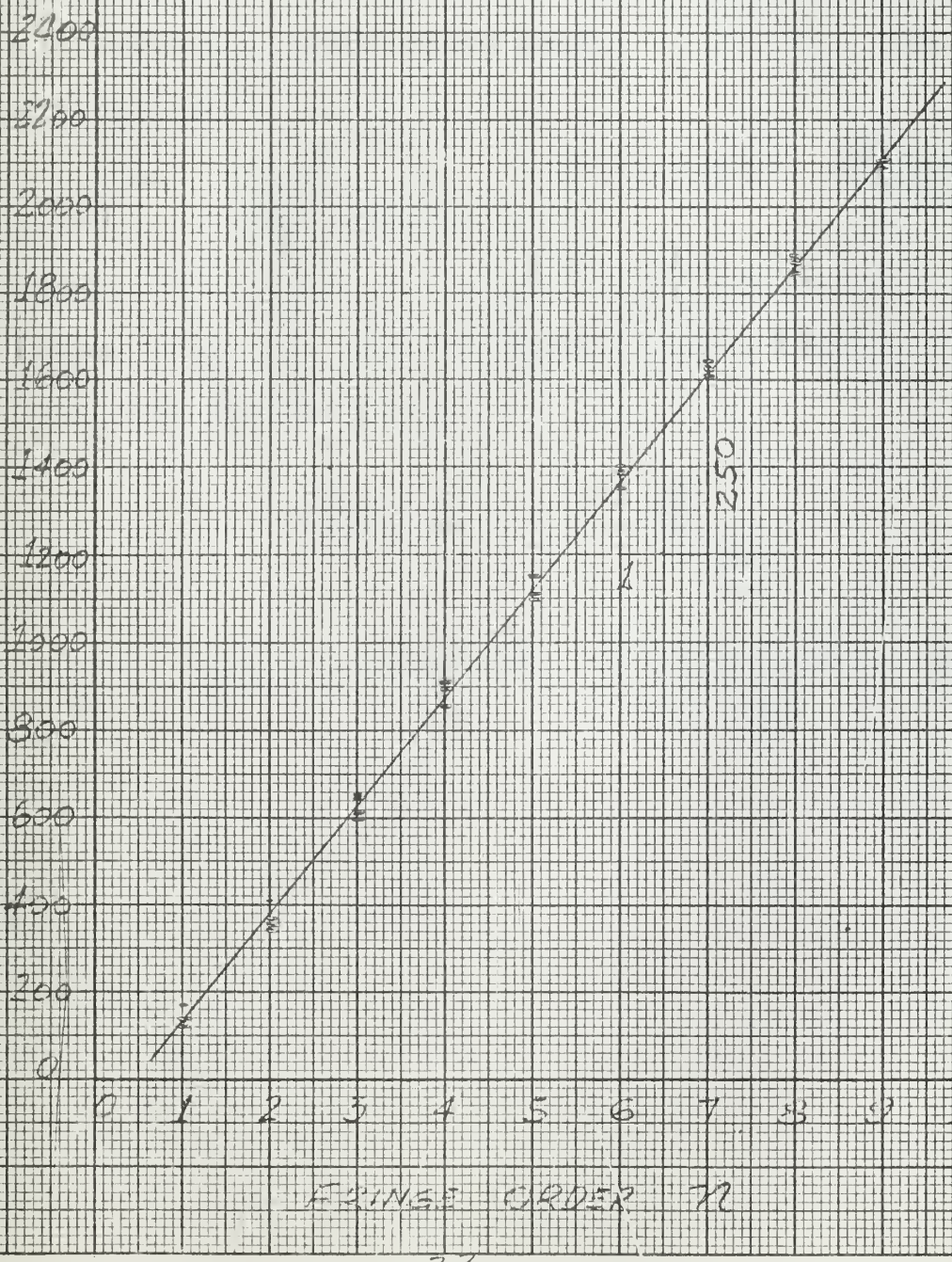

Calculations

Referring to Eq. 1 and solving for the material fringe value C yields

$$C = \frac{n\lambda}{\delta(\sigma_1 - \sigma_2)}$$

Substituting for λ, the wavelength of the monochromatic green light used (5461 Å = 21.5×10^{-6} inches); for the thickness δ, the depth of the tension model (0.315 inches); and for $n/(\sigma_1 - \sigma_2)$, the data derived from Fig. 13 (1/'50):

$$C = \frac{21.5 \times 10^{-6}}{(.315)(250)} = 27.3 \times 10^{-8} \ \frac{\text{fringe}}{\text{psi}}$$

Equating the right hand sides of Eqs. 1 and 2, substituting for $\epsilon_1 - \epsilon_2$ in terms of $\sigma_1 - \sigma_2$, and solving for the material fringe value in terms of the principal strains

$$K = C\frac{E}{1+\mu}$$

$$K = 27.3 \times 10^{-8} \ \frac{445{,}000}{1 + .46} = 8.31 \times 10^{-2} \ \frac{\text{fringe-inch}}{\text{inch}}$$

Appendix II

Photostress Type A Liquid Plastic

A Determination of Modulus of Elasticity, Shear Modulus, and Poisson's Ratio

For this experiment, a simple, rectangular section tension model of dimensions 0.375" x 0.315" x 6" was cast and machined to size. The upper end of the model was placed in and supported by clamp type jaws while the lower end was loaded with a dead weight system. Strains in the longitudinal and lateral directions were observed by means of Tuckerman optical strain gages for each known increment of load. The strain gages were arranged on opposite faces of the tension model and held in place with rubber bands. The gage measuring longitudinal strain had a one inch gage length while the lateral gage had a 1/4 inch gage length. Strains indicated by the optical strain gages were observed through autocollimators. The behavior of the plastic was essentially linear up to the maximum stress attained, 1872 psi.

Experimental data, charts, and calculations are shown on the following pages.

Data

Photostress Type A Liquid Plastic--15 per cent Hardener by Weight. Tension Test to Determine Modulus of Elasticity and Poisson's Ratio

Area = 0.1182 in.^{2}

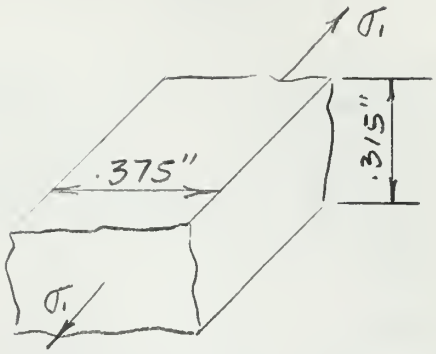

Fig. 14 Tension Model Dimensions

Run I (Autocollimator Factor 1.003)

Load pounds	σ_1 psi	Longitudinal Gage Reading Gage No. 851 1" Gage Length Gage Factor 1.995	Lateral Gage Reading Gage No. 854 1/4" Gage Length Gage Factor 8.020
0	0	- - - -	12.80
25.9	219	2.64	12.52
51.0	431	4.24	12.16
77.6	656	6.40	11.80
102.6	866	8.78	11.66
127.8	1080	11.02	11.38
152.9	1292	13.56	----
177.9	1502	16.14	----
221.8	1872	20.76	----

Run II (Autocollimator Factor 1.003)

Load pounds	σ_1 psi	Longitudinal Gage Reading Gage No. 851 1" Gage Length Gage Factor 1.995	Lateral Gage Reading Gage No. 854 1/4" Gage Length Gage Factor 8.020
0	0	3.34	16.58
25.9	219	3.74	16.26
51.0	431	5.40	16.00
77.6	656	7.48	15.62
102.6	866	9.82	15.44
127.8	1080	12.08	15.18
152.9	1292	14.72	14.80
177.9	1502	17.08	14.54
199.9	1690	19.36	14.44
221.8	1872	21.66	14.20

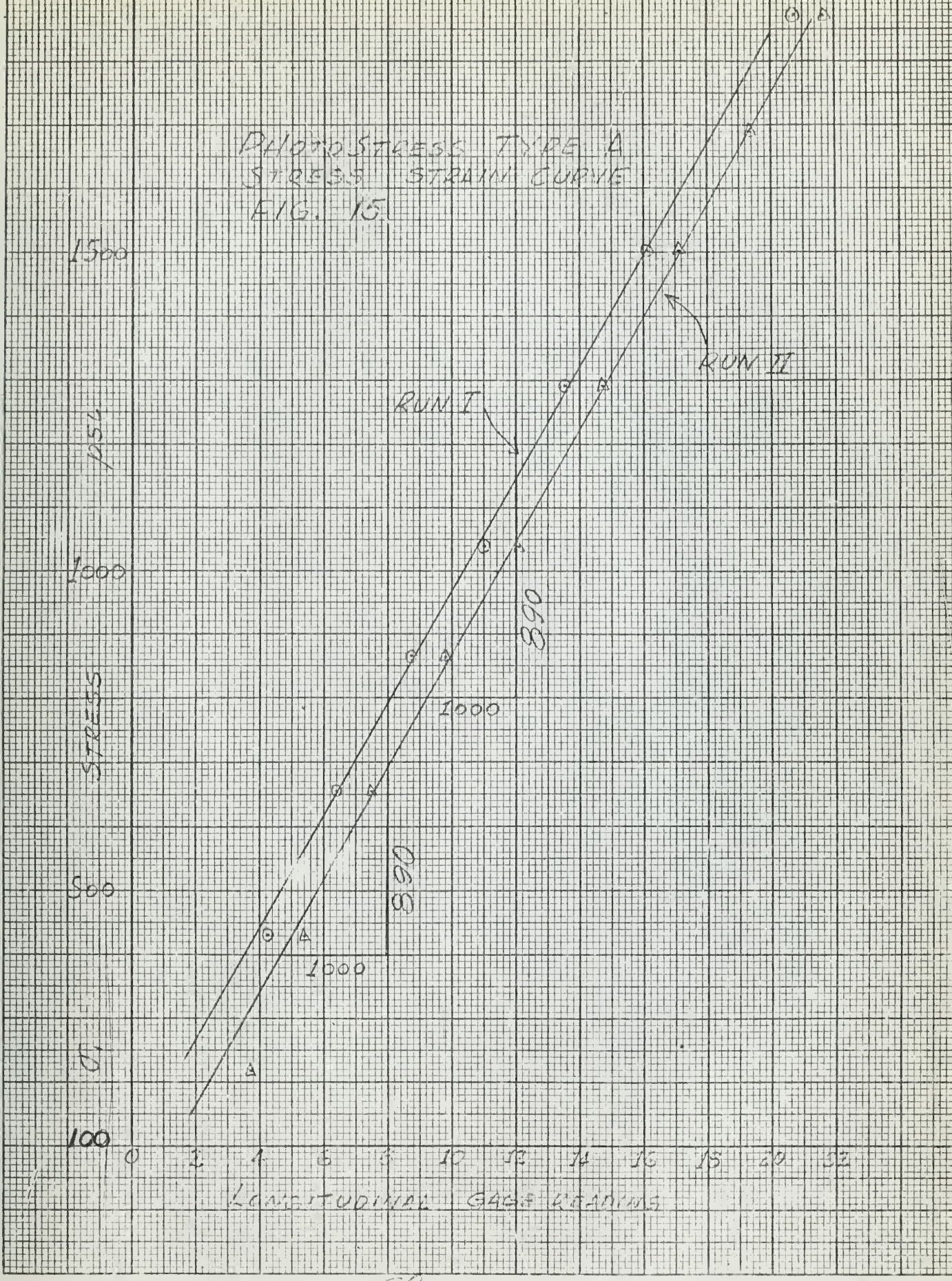
PILOT STEEL TYPE A
STRESS STRAIN CURVE
FIG. 15
RUN I
RUN II
890
1000
890
1000
STRESS
1500
1000
500
0
100
0
1
2
4
6
8
10
12
14
16
18
20
22
LONGITUDINAL GAGE READINGS

PHOTOSTRESS TYPE A
STRESS STRAIN CURVE
FIG. 16

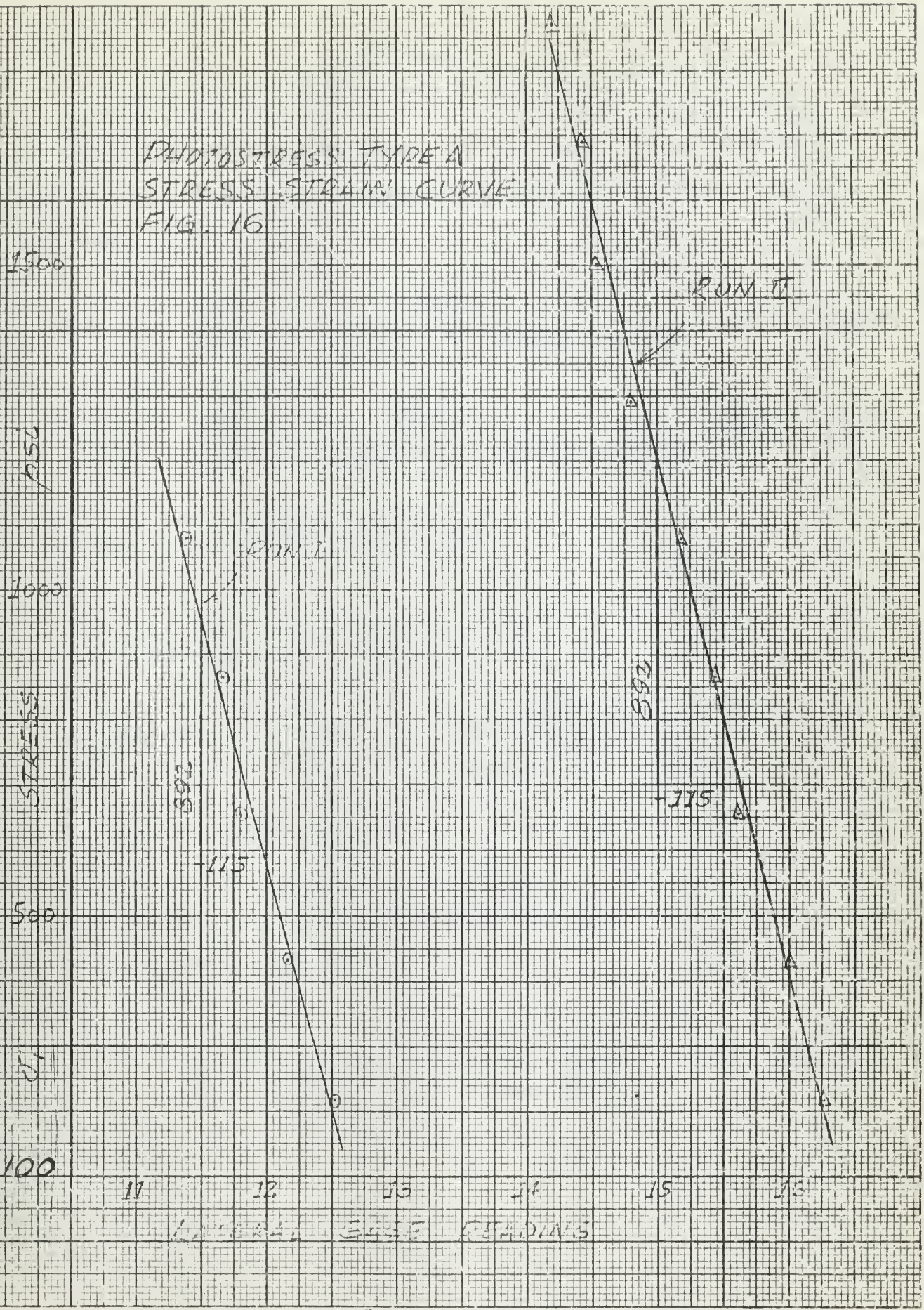

Calculations

The average value of the slopes of the stress vs. strain curves plotted in Fig. 15 gives the modulus of elasticity of Photostress Type A plastic.

$$E_I = \frac{\Delta\sigma_1}{\Delta\epsilon_1} = \frac{890}{1000^{-6}(1.995)(1.003)} = 445{,}000 \text{ psi}$$

$$E_{II} = \frac{\Delta\sigma_1}{\Delta\epsilon_1} = \frac{890}{1000^{-6}(1.995)(1.003)} = 445{,}000 \text{ psi}$$

$$E_{AVG} = 445{,}000 \text{ psi}$$

Poisson's ratio, μ is then defined by

$$\mu = \frac{-\epsilon_2}{\epsilon_1} = \frac{-(-115^{-6})(8.020)(1.003)}{1000^{-6}(1.995)(1.003)}$$

$$\mu = 0.46$$

ϵ_2 is obtained from the stress vs. strain curves of Fig. 16. Finally, the shear modulus G can be found.

$$G = \frac{E}{2(1+\mu)} = \frac{445{,}000}{2(1+.46)} = 152{,}000 \text{ psi}$$

Appendix III

Molding and Contouring the Photostress Plastic Sleeve

Liquid Photostress is a thermoplastic (polyester) which is received and stored with a separate hardener.[1] Storing at temperatures of 40°F or lower prolongs shelf life indefinitely. The liquid plastic is most conveniently prepared for use in a container of approximately eight ounce capacity. Upon pouring, air bubbles become entrapped in the viscous liquid. These air bubbles, present in sufficient quantity, distort a stress-optic pattern. In general, it is best to heat the plastic to 140-160°F until the bubbles disappear. Allowing it to cool to room temperature and combining with 15 per cent hardener by weight, the mixture is combined thoroughly, but slowly (so as not to entrap more bubbles), until an exothermic reaction accompanied by a temperature rise to 110°F is observed. The mixing time was found to be in the order of 25 minutes and a Weston dial thermometer found convenient for observing temperature. The importance of thorough mixing cannot be overemphasized since failure to do so will result in an ineffective and incompletely polymerized sheet (Fig. 17).

At 110°F the plastic is ready and must be immediately poured into a prepared mold. All parts of the mold should be coated with silicone varnish cured at 400-500°F for four hours. The silicone insures easy removal of the plastic sheet from the mold. Tatnall recommends a controlled atmosphere with relative humidity lower than 45 per cent while the plastic

---

[1] Tatnall Measuring Systems Company Bulletins pertaining to use, procedures in handling, and selection of Photostress type. See Bibliography.

is curing. This becomes more important as the area of the plastic exposed to the atmosphere is increased. Humid conditions will produce a broken, paraffin like film on the surface of the sheet being prepared and this film will distort a stress-optic pattern (Fig. 18). If the mold is arranged so that only a small area is exposed (one inch^2, say), humidity seems to present no problem. If necessary, dampness may be controlled by the use of an oven, infra-red lamps, or chemical humidity absorbers. Heat may be used to reduce curing time; time required at 100°F was found to be approximately one half that required at room temperature (two hours).

Curing is not completed in the mold. When the plastic has reached the stage where the surface may be indented with a knife point without adhering to the blade, and the indentation heals, the sheet is ready for removal and contouring to the work piece. The proper stage of curing must be awaited carefully. Premature removal destroys the sheet, while late removal induces strains which produce permanent double refraction. An adhesive, supplied and prepared in advance, is used to bond the sheet. The pressure applied to hold the plastic in place during the final stages of curing should be sufficient to maintain contact between sheet and part. A cellulose sponge or clear cellophane tape was found convenient for this purpose. Parts to which the plastic is applied must be thoroughly degreased. Acetone is recommended.

Photostress sheets from 0.048 inches to 0.084 inches will readily conform to a one-half inch radius of curvature; sheets from 0.084 inches to 0.120 inches thick will conform to a one inch radius. The tapered sleeve originally prepared for this project was cast on a silicone treated glass plate on which was placed a hollow, rectangular sectioned metal dam. The glass plate was in turn placed on a metal plate supported by

equilaterally arranged leveling screws (Fig. 19). This entire assembly was then tilted to enable a sheet of variable thickness to be cast. This method, while useable for certain applications, proved unsuccessful for contouring a sheet of desired proportions to a one inch diameter aluminum tube. The sleeve or sheet, increasing in thickness from 0.048 inches, to 0.120 inches over a one and one-half inch length, was extremely difficult to contour and maintain in position while bonding. Difficulty was also encountered in making a continuous seam.

Photostress, completely cured, is easily machined. No noticeable stresses are induced in the finished product, if reasonable care is taken and the plastic is machined slowly. A satisfactory sleeve was made by casting the liquid plastic directly into a suitable right circular cylindrical mold mounted on a one inch diameter tube. The plastic was allowed to cure completely at room temperature. The fiber composition mold was then machined off leaving a plastic sleeve of uniform thickness bonded to the tube. This, in turn, was machined to the desired shape. Mineral oil was used as a cooling agent while machining, and was also used to maintain a seal on machined surfaces and ends of sleeve to prevent moisture seepage.

Working with liquid Photostress requires some technique, but once a familiarity with it is acquired, surprisingly little time is spent in preparing a work part for test. Twenty four hours should always be allowed from application to testing. Edge effects were apparent over one quarter inch of the sleeve ends, and consequently, readings could not be taken in this area.

Various shapes were tried; the dimensions shown in Fig. 5 were

adopted as the most satisfactory. Trial sleeves with a smaller taper tended to disperse the stress-optic pattern making it more diffuse and difficult to analyze quantitatively. Sleeves with a greater degree of taper produced a more satisfactorily defined pattern. The dimensions adopted produced adequate response to principal stress differences, and at the same time, gave a sleeve long enough to reduce, to a minimum, the inevitable experimental error in locating fringes.

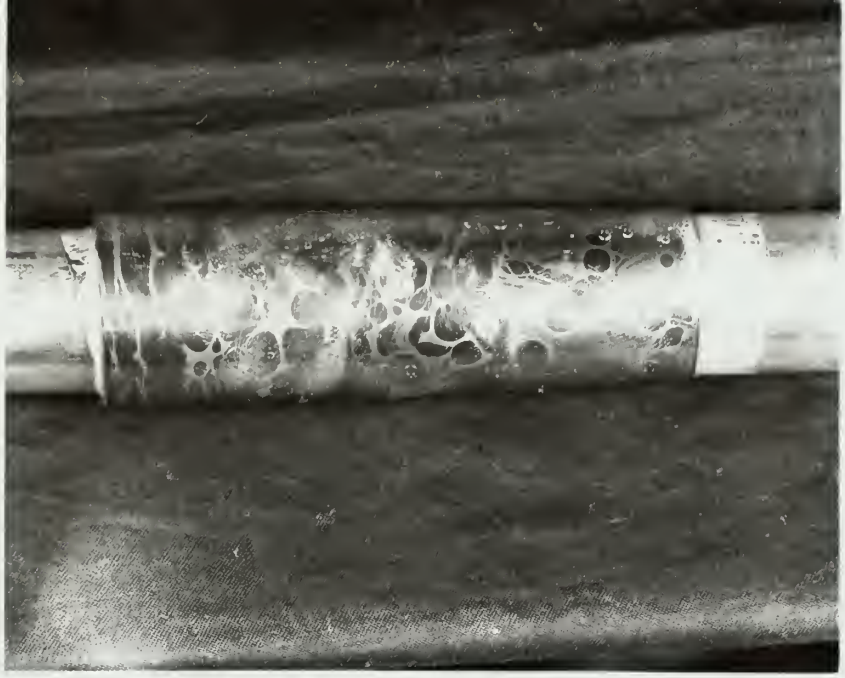

Fig. 17 The effects of incomplete polymerization on Photostress Plastic

Fig. 18 The effects of humidity on Photostress Plastic in the curing stage.

Fig. 19 Tension Models used are shown with suitable equipment for casting contoured sheets. The infra-red lamp was used to reduce curing time and control himidity.